AUTOMATED DETECTION OF PELVIC FRACTURES FROM VOLUMETRIC CT IMAGES

Ananda S. Chowdhury[1], Joseph E. Burns[2,3], Arka Mukherjee[1], Bhaskar Sen[1], Jianhua Yao[2], Ronald M. Summers[2]
{aschowdhury@etce.jdvu.ac.in, jburns@uci.edu, (arkamukherjee49, bhaskarsen.ju)@gmail.com, jyao@cc.nih.gov, rms@nih.gov}

[1]Dept. of Electronics & Telecom. Engineering
Jadavpur University,
Kolkata -700032, India.

[2]Dept. of Radiology and Imaging Sciences
National Institutes of Health, Clinical Center
Bethesda, MD 20892-1182, USA.

[3]Dept. of Radiological Sciences
University of California, Irvine
Irvine, CA 92697, USA.

ABSTRACT

Pelvic fractures are a major cause of trauma patient mortality. Detection and management of pelvic injuries is challenging due to myriad injury patterns and associated complications such as hemorrhage and infection. In this paper, we propose an automated method of pelvic fracture detection from volumetric CT images. A coarse-to-fine strategy is adopted where a potential region containing the fracture is identified first using intensity and curvature information. The above region is modeled as a weighted graph and a fracture is modeled as a minimum cut in this graph. A second localizing algorithm models the same fracture as a valley, based on the signs of the mean and Gaussian curvature. The minimum cuts as well as the spatial consistent valleys, in isolation, generate a small number of false positives in addition to the true fracture. A joint decision process based on the volumetric graph cuts and the spatially consistent valleys eliminates the false positives. Experimental results indicate the effectiveness of the proposed scheme.

Index Terms— Pelvic fracture, Graph Cut, Mean and Gaussian curvatures.

1. INTRODUCTION

Traumatic injury of the pelvis is a frequently encountered pathology, and pelvic fractures are a major cause of trauma patient mortality [1]. Detection and management of pelvic injuries can be a challenge, as manifold injury patterns may occur, with varying degree of complications such as hemorrhage and infection. Associated with high energy impact forces, pelvic fractures have significant association with internal organ injuries [2-3]. Where only approximately 3% of skeletal system fractures occur in the pelvis, they are associated with mortality rates of 10-16% [4]. The overall goal is to develop an efficient and rapid CAD system for pelvic fractures. This system has the potential to improve the speed and sensitivity for fracture detection, and increase the accuracy of delineation of fracture anatomy, in trauma patients at an early stage post injury when they are most amenable to intervention and improved prognosis. Here, we focus on basic constituent or elemental "sub-fractures" that in combination make up the more global pelvic fracture patterns as pieces in a puzzle.

Computer aided segmentation of pelvic bones using Laplacian filtering and morphological operations can be found in a work of Vasilache *et al.* [5]. A related work on the segmentation of acetabulum and femoral head bones in 3D is proposed by Zoroofi *et. al.* [6]. Fornaro *et. al.* discusses graph cut-based semi-automated segmentation of fractured pelvic bones [7]. Detection of fractures appearing exclusively in the pelvic ring using discrete wavelet transform is reported by Smith *et. al.* [8]. Wu *et al.* reported using adaptive windowing, boundary tracing, wavelet transform, and anatomical information, for pelvic fracture detection in 2D CT slices [9]. This method of fracture detection uses a "segmentation-followed-by-registration" strategy which makes it computationally intensive. Chowdhury *et. al.* showed a less computationally intensive semi-automated detection of pelvic fractures in 2D CT slices [10]. However, in [10], user has to manually delineate a region surrounding the fracture. Graph cuts [11] and curvature analysis [12] are then employed to detect a fracture. A fracture is first modeled as a minimum cut in an appropriately weighted graph. The same fracture is then modeled as a "valley surface" (mean curvature (H) > 0 and Gaussian curvature (K) = 0). A combination of graph cuts and valleys, followed by some heuristic neighborhood analysis is used to finally detect the fracture.

Coarse-to-fine strategies are commonly used for segmentation and tracking problems [13]. The current paper proposes a coarse-to-fine approach for fracture detection from volumetric CT and specifically enhances the work described in [10] with three distinct and significant improvements. First, coarse localization of fractures is achieved using measures of intensity and curvature without any user intervention. Second, we extend the work in [10] to volumetric CT images with necessary modifications. The modifications include application of the graph cut algorithm on an appropriately constructed 3D graph and enforcement of spatial constraints on the already detected "valley surfaces" in individual 2D slices. Third, we eliminate the final post-processing step in [10] and hence make our method more robust. A joint decision from the volumetric graph cuts and the spatially constrained valleys is shown to be sufficient to capture only the true fractures.

2. METHODS

In this section, we describe our proposed method of fracture detection. Fig. 1 shows the flowchart of our method.

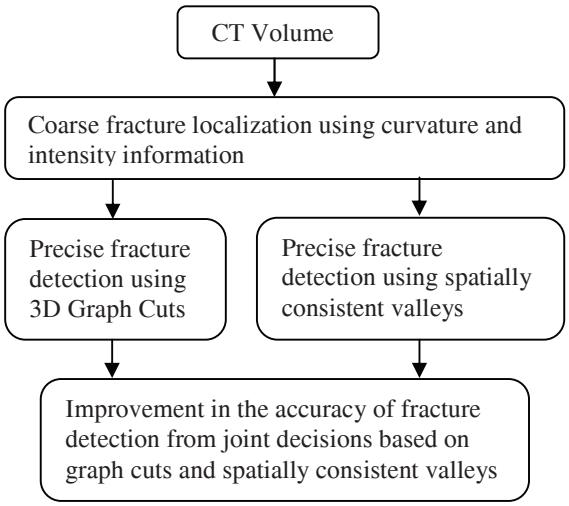


Fig. 1. Flowchart for the proposed method

2.1. Coarse Fracture Localization

We divide the input pelvic CT volume data into several disjoint small volumetric regions (henceforth will be simply called region(s)), i.e., $V = \bigcup_{i=1}^{n} R_i, R_i \bigcap R_j = \phi$, where ϕ denotes a null set. The goal here is to automatically identify the region(s) (R_i) containing the fracture based on certain specific characteristics. Two measures, one based on the intensity pattern and the other based on the curvature profile are used to characterize all the disjoint regions. Use of disjoint regions makes overall computation less intensive and characterization more distinct. Firstly, a fracture is defined here as a volume devoid of bone density and structure, bordered by bone on at least two non-contiguous sides. In CT scans, a fracture site is thus characterized by a few voxels with low intensity (loss of bones) surrounded by a large number of voxels with high intensity (bones). Hence, a region containing fracture should exhibit high average intensity locally. Secondly, any local surface can be classified into one of the eight surface primitives based on the values of the mean (H) and Gaussian (K) curvature. Fracture sites are geometrically modeled as "valley surface(s)" (henceforth will be simply called valleys). Two (2x2) matrices called the First Fundamental Form matrix **G** and the Second Fundamental Form matrix **B** are used to describe such surfaces**.** The principal curvatures (κ_1 and κ_2) are the roots of the following quadratic equation [12]:

$$|G|k_n^2 - (g_{11}b_{22} + b_{11}g_{22} - 2g_{12}b_{12})\kappa_n + |B| = 0\,;\; n = 1, 2 \quad (1)$$

where |G| and |B| denote the magnitudes of the determinants of the matrices **G** and **B** respectively. The mean and Gaussian curvatures can be respectively expressed in terms of the principal curvatures (κ_1 and κ_2) as follows:

$$H = (\kappa_1 + \kappa_2)/2 \quad (2a)$$

$$K = \kappa_1\kappa_2 \quad (2b)$$

Any pixel on the intensity surface with $K = 0$ and $H > 0$ is labelled as a valley. Note that a deep valley is marked by a high value of Mean curvature. Since fracture sites contain deep valleys, we add the mean curvature values of all the valley pixels in a region. A region containing a fracture should exhibit a large value of the sum of mean curvatures. In fact, the product of average intensity and the sum of mean curvatures is used as the measure, denoted by $M(R_i)$, to determine the region(s) containing fracture. Let n_i and m_i be the number of voxels and number of valleys in R_i respectively. H_{ij} denotes the mean curvature of j^{th} valley in R_i. Furthermore, there are n_{ik} voxels in R_i having intensity I_{ik} and there are q distinct intensities. So, we can write:

$$M(R_i) = \left(\frac{\sum_{k=1}^{q} n_{ik} I_{ik}}{n_i}\right) * \left(\sum_{j=1}^{m_i} H_{ij}\right) \quad (3)$$

R_i's are now sorted in the descending order based on the values of $M(R_i)$. Only top p of them are chosen as potential fracture containing regions.

2.2. Precise Fracture Detection using 3D Graph Cuts

The localized region is modeled as a weighted undirected 3D graph $G_{3D}(V_{3D},E_{3D})$. Each voxel v in this region is a node/vertex in G_{3D}. Two special terminal nodes, called the 'source'(s) and the 'sink'(t) are respectively formed from the "object" seeds and the "background" seeds (provided by the user). The t-links connect all the individual pixels v to the source node s and the sink node t. We use a complete first-order 3D neighborhood. The n-links are constructed between each voxel v and its 26 neighbors. So, we can write: $V_{3D} = Vx \bigcup s \bigcup t$ and $E_{3D} = T \bigcup N$. Here, Vx denotes the set of voxels within the localized region. A flow network is considered, where a minimum cut set would constitute edges across the "object" (bony structures with high intensities) class and the "background" (fracture plus soft tissues with low intensities) class. Cut vertices of the "background" class will contain the potential fracture points. Ford-Fulkerson algorithm is employed in this work to find a minimum cut. The graph cut energy function for any segmentation A is given by:

$$E(A) = B(A) + \lambda R(A) \quad (4)$$

where the boundary properties are given by the term $B(A)$ and the region properties are given by the term $R(A)$. Mathematically, they can be expressed as:

$$B(A) = \sum_{v,w \in Ne(v)} B_{\{v,w\}} \quad (5)$$

$$R(A) = \sum_{v \in Vx} R_v(A_v) \quad (6)$$

Let O, B and I_v be the histogram of the object seeds, the histogram of the background seeds and the intensity of any voxel v, respectively. Further, let $Pr(I_v|O)$ and $Pr(I_v|B)$ denote the probability of a certain voxel v to belong to the class "object" and to the class "background" respectively.

We now define $B\{p,q\}$, R_v(*"object"*) and R_v(*"background"*) in the following equations [11]:

$$B_{\{v,w\}} \propto \exp(-(I_v - I_w)^2 / 2\sigma^2) * (d(v,w))^{-1} \quad (7)$$

$$R_v(\text{"}object\text{"}) \propto \ln(\Pr(I_v \mid O)) \quad (8)$$

$$R_v(\text{"}background\text{"}) \propto \ln(\Pr(I_v \mid B)) \quad (9)$$

The terms I_v (I_w) and $d(v,w)$ respectively denote the intensity of the voxel v (w) and the distance between the two voxels v and w. In the chosen neighborhood system, $d(v,w)$ can vary between 1 and √3. The augmenting paths in the Ford-Fulkerson algorithm are detected using breadth-first-search following Edmonds and Karp [14]. So, the complexity of the max-flow min-cut algorithm becomes $\boldsymbol{O(V_{3D}E_{3D}^2)}$.

2.3. Precise Fracture Detection using Spatially Consistent Valleys

Since a fracture can be modelled as a valley, all the valleys in each 2D slice are detected first. Curvature computation is inherently noisy, so a small number of spurious valleys are also detected in the process. A true fracture spans several slices in the CT volume. So, we enforce a spatial consistency check over consecutive slices where the fracture can be observed properly, on the already detected valleys. If a particular valley is detected in several slices, then we deem it spatially consistent.

2.4. Fracture Detection from Joint Decision

We now create a joint fracture candidate set, which is formed by the intersection of the individual decision sets of fracture candidates obtained using the graph cut and curvatures methods described above. Thus, a voxel is inferred to be a fracture if i) it is a cut point in a 3D graph and ii) it is a spatially consistent valley. Through this joint decision process false positives are eliminated.

3. EXPERIMENTAL RESULTS

We experimented with 5 CT volumes, obtained from the University of California, Irvine Medical Center with varying resolutions (0.63 - 0.83 mm/pixels). Each case contains a single fracture. The pelvic fractures for the 5 cases appear at different locations, e.g., on the left sided transverse process of the L5 vertebral body (shown in fig. 4(d)), right inferior public ramus and left sided periacetabular region of the pelvis. Matlab BGL [15] is used for implementing the Edmonds-Karp algorithm. For the fracture localization, 60 pixels x 60 pixels regions are used and only the top 2 regions are chosen (i.e., p=2). For the graph cut, we experimentally set the parameters λ = 80 and σ = 6. For the curvature-based approach, we experimentally set the optimum kernel size to 9 x 9 pixels. All the parameters, once chosen, are kept constant throughout. The ground-truth is obtained through manual marking of fracture points in various slices in the CT stack by the domain experts. We now first show the effectiveness of the term $M(R_i)$ for fracture localization. Four different regions are shown in fig. 2 and the value of $M(R_i)$ for each of them is given in table 1. In fig. 3, we graphically show the value of $M(R_i)$ for all the regions in fig. 2. Only top 2 regions (C and D in fig. 2) are selected as the ones containing the fracture. The rationale behind choosing two regions (i.e., p=2) is that a fracture may not be contained in a single region. In fact, figures 2 and 4(d) indicate that the fracture point falls on the boundary of the regions C and D.

Table 1. Value of $M(R_i)$ for four different regions in fig. 1

R_i	Average Intensity	Sum of Mean Curvatures at Valleys	$M(R_i)$
A	53.66	118.93	6381.78
B	227.04	56.38	12800.51
C	**220.26**	**93.5**	**20594.31**
D	**220.83**	**91.65**	**20239.06**

Table 1 clearly demonstrates why both the average intensity and the sum of mean curvatures are needed for coarse fracture localization. Precise fracture detection methods are applied on the entire region constituted by C and D.

Table 2. Performance of various fracture detection methods

Method	Sensitivity (%)	Specificity (%)
3D Graph cut	100	$\frac{17075}{17075 + 920} = 95$
Spatially Consistent Valley	100	$\frac{16178}{16178 + 1817} = 90$
Joint Decision	100	$\frac{17995}{17995 + 0} = 100$

Volumetric graph cuts and spatially consistent valleys individually and in combination can detect the single fracture voxel in all slices in all cases. So, there is no false negative voxel and *sensitivity* of all the methods is 100%. However, both the graph cuts and the spatially consistent valleys, when run in isolation, detect some false positive voxels. This can be seen from the specificity values in Table 2 and false positive pixels in fig. 4(a) and 4(b). Since the numbers of true negatives largely outweigh the number of false positives, moderately high values of specificity are obtained for volumetric graph cuts and spatially consistent valleys. The optimal detection resulting from the joint decision process, where *specificity* is improved to 100%, is shown in fig. 4(c). Fig. 4(c) also appears closest to the ground-truth in fig. 4(d). Note that a detected fracture point is marked as correct if it coincides with the ground-truth point or falls within a distance of 5 pixels (value set from the domain knowledge) from the ground-truth point. Fractures are displayed in 2D cross sections (fig. 4) in parallel with the current standard by which fractures are detected and assessed in clinical practice. These images allow a higher level assessment of the internal structural detail and anatomical involvement of the fractures. The proposed methods on average take 30 seconds to execute on an Intel(R) Core(TM)2 Duo processor with a speed of 2.8 GHz.

4. CONCLUSION AND FUTURE WORK

In this paper, automated detection of pelvic fractures in volumetric CT images is discussed. A coarse-to-fine strategy is adopted for that purpose. During the coarse fracture localization phase, average intensity and sum of mean curvatures for valleys are employed. In the precise detection phase, a joint decision process based on the volumetric cuts and spatially consistent valleys are used to identify the fracture voxels. In future, we will use anatomical models to distinguish between fractures and normal gaps between bones, such as joints. In addition, we will evaluate the performance of the present fracture detection approach on a large and more diverse database containing single or multiple pelvic fractures.

Acknowledgement

This research was supported in part by the Imaging Sciences Training Program sponsored by the Radiology and Imaging Sciences Department and the National Institute of Biomedical Imaging and Bioengineering of the National Institutes of Health. This research was also supported in part by the National Institutes of Health Clinical Center.

REFERENCES

[1] L.C. Chien, H.M. Cheng, W.C. Chen, and M.C. Tsai, "Fracture and Risk Factors for Mortality: A Population-Based Study in Taiwan", *Eur J Trauma Emerg Surg*, 36:131-137, 2010.

[2] D. Demetriades, M. Karaiskakis, K. Toutouzas, K. Alo, G. Velmahos, and L. Chan, "Pelvic Fractures: Epidemiology and Predictors of Associated Abdominal Injuries and Outcomes", *Am Coll Surg*, 195:1-10, 2002.

[3] S.J. Slater, and D.A. Barron, "Pelvic fractures—A guide to classification and management", *European Journal of Radiology*, 74(1):16-23, 2010.

[4] M.R. Grotz, M.K. Allami, P. Harwood, H.C. Pape, C. Krettek, and P.V. Giannoudis, "Open pelvic fractures: epidemiology, current concepts of management and outcome", *Injury*, 36(1): 1-13, 2005.

[5] S. Vasilache and K. Najarian, "Automated Bone Segmentation from Pelvic CT images", *Proc. IEEE Wkshp. on Bioinformatics and Biomedicine (BIBMW)*, Philadelphia, PA, 41-47, 2008.

[6] R. A. Zoroofi, Y. Sato T. Sasama, t. Nishii, N. Sugano, K. Yonenobu, H. Yoshikawa, T. Ochi, and S. Tamura, "Automated Segmentation of Acetabulum and Femoral Head from 3D CT images", *IEEE Trans. Inf. Tech. in Biomedicine*, 7(4): 329-343, 2003.

[7] J. Fornaro, G. Szekely, and M. Harders,"Semi-automatic Segmentation of Fractured Pelvic Bones for Surgical Planning", *Proc. Int. Symp. on Biomedical Simulation (ISBMS)*, Springer LNCS 5958: 82-89, 2010.

[8] R. Smith, K. Ward, C. Cockrell, J. Ha and K. Najarian, "Detection of Fracture and Quantitative Assessment of Displacement Management in Pelvic X-ray Images," *Proc. IEEE Conf. on Acoustics Speech and Signal Processing (ICASSP)*, 682-685, 2010.

[9] J. Wu, P. Davuluri, K. Ward, C. Cockrell, R. Hobson, and K. Najarian, "Fracture Detection in Trauma Pelvic CT Images", *Int. J. Biomed. Imaging,* pp. 1-16, 2011.

[10] A.S. Chowdhury, J. Burns, B. Sen, A. Mukherjee, J. Yao and R.M. Summers, "Detection of Pelvic Fractures using Graph Cuts and Curvatures", *Proc. IEEE Int. Conf. on Image Processing (ICIP)*, 1605-1608, 2011.

[11] Y. Boykov and M.P. Jolly, "Interactive Graph Cuts for Optimal Boundary and Region Segmentation of Objects in N-D Images," *Proc. IEEE Conf. on Computer Vision (ICCV)*, Vancouver, Canada, 105-112, 2001.

[12] Bhandarkar S.M. and M. Suk, "Object Recognition from Range Images", Springer-Verlag Inc., Tokyo, Japan, 1992.

[13] G. Sundarmoorthi, A. Yezzi, and A.C. Mennucci, "Coarse-to-Fine Segmentation and Tracking Using Sobolev Active Contours", *IEEE Trans. Pattern Anal. Mach. Intell.*, 30(5), 851 – 864, 2008.

[14] J. Edmonds and R.M. Karp, "Theoretical improvements in algorithmic efficiency for network flow problems", *Journal of the ACM*, 19(2), 248-264, 1972.

[15] http://www.stanford.edu/~dgleich/programs/matlab_bgl/

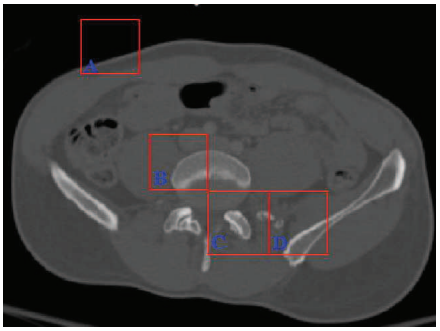


Fig. 2. Four different regions for fracture localization

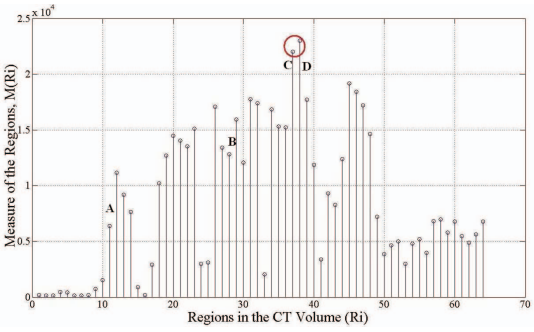
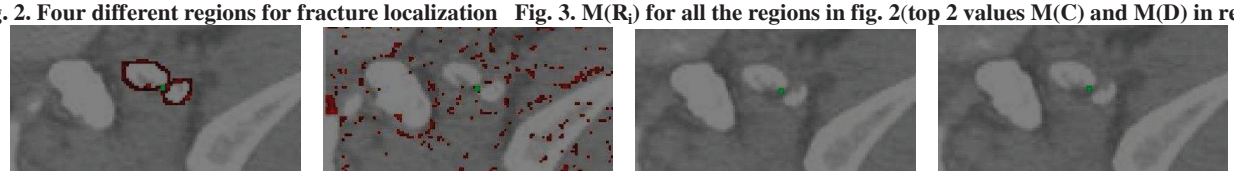


Fig. 3. M(R_i) for all the regions in fig. 2(top 2 values M(C) and M(D) in red)



(a) (b) (c) (d)

Fig. 4: Fracture detection within the region constituted by C and D (zoomed) (a) graph cut, (b) spatially consistent valleys, (c) combining (a) and (b), (d) Ground truth [Correct Fracture: Green, Incorrect Fracture: Red]